Published in final edited form as:
Magn Reson Med. 2008 April ; 59(4): 747–754. doi:10.1002/mrm.21530.

Differentiation between Benign and Malignant Breast Lesions Detected by Bilateral Dynamic Contrast-Enhanced MRI: A Sensitivity and Specificity Study

Sanaz A. Jansen, **Xiaobing Fan**, **Gregory S. Karczmar**, **Hiroyuki Abe**, **Robert A. Schmidt**, and **Gillian M. Newstead***
Department of Radiology, University of Chicago, Chicago, Illinois

Abstract

The purpose of this study was to apply an empirical mathematical model (EMM) to kinetic data acquired under a clinical protocol to determine if the sensitivity and specificity can be improved compared with qualitative BI-RADS descriptors of kinetics. 3D DCE-MRI data from 100 patients with 34 benign and 79 malignant lesions were selected for review under an Institutional Review Board (IRB)-approved protocol. The sensitivity and specificity of the delayed phase classification were 91% and 18%, respectively. The EMM was able to accurately fit these curves. There was a statistically significant difference between benign and malignant lesions for several model parameters: the uptake rate, initial slope, signal enhancement ratio, and curvature at the peak enhancement (at most $P = 0.04$). These results demonstrated that EMM analysis provided at least the diagnostic accuracy of the kinetic classifiers described in the BI-RADS lexicon, and offered a few key advantages. It can be used to standardize data from institutions with different dynamic protocols and can provide a more objective classification with continuous variables so that thresholds can be set to achieve desired sensitivity and specificity. This suggests that the EMM may be useful for analysis of routine clinical data.

Keywords

malignant; breast; DCE-MRI; sensitivity

INTRODUCTION

Improvements in breast cancer detection are largely responsible for increasing survival among breast cancer patients (1). Dynamic contrast-enhanced MRI (DCE-MRI) is being used in breast imaging for several purposes, including determining extent of malignant disease and posttreatment evaluation (2,3). DCE-MRI has a high sensitivity to breast cancer, with a lower specificity (4–6). When analyzing DCE-MRI the radiologist assesses both the lesion morphology and kinetics of contrast enhancement. Some studies have suggested that the morphologic information from DCE-MRI is more diagnostically useful than the kinetic information (7,8), implying that there may be room for improvement in extracting more diagnostically relevant information from kinetic data.

Ideally, DCE-MRI protocols would acquire data with high spatial and high temporal resolution to fully exploit both the morphologic and kinetic information. Unfortunately, with

*Correspondence to: Gillian Newstead, MD, Department of Radiology, University of Chicago, 5841 S. Maryland Ave., MC 2026, Chicago, IL 60637. gnewstead@radiology.bsd.uchicago.edu.

currently available equipment and techniques there is always a trade-off between spatial and temporal resolution in DCE-MRI (7). As a result, the signal intensity versus time—or kinetic—curves typically have only 3–7 data points (9–11) for 3D DCE-MRI, which presents a challenge for differentiating benign from malignant lesions. To simplify analysis of the kinetic curves, radiologists qualitatively assess the initial rise and delayed phase according to the BI-RADS lexicon. Several reports have demonstrated that DCE-MRI data from malignant lesions tend to exhibit "washout" curves, while benign lesions tend to show persistent signal increase with time after contrast injection (12,13). Some groups have performed semiquantitative analysis of these curves—for example, calculating the time to peak enhancement—to better distinguish between the benign and malignant lesions (10). However, semiquantitative parameters have limited use since they are susceptible to errors due to noise, and with varying timing of acquisitions across institutions comparison of these parameters between institutions is problematic.

There have been several studies of pharmacokinetic compartment modeling on breast 3D DCE-MRI data, to relate kinetic curves to the underlying physiology of the lesions (14–18). However, for low time resolution 3D DCE-MRI data the accuracy of physiological parameters obtained from compartmental models is questionable. In addition, these models require an arterial input function (AIF), which is difficult to estimate accurately. As an alternative to these approaches, mathematical equations can be used to fit the kinetic curves. For example, Heiberg et al. (19) used a fifth-order polynomial to fit the kinetic curves (5–7 points), but the coefficients of the polynomial did not show a significant difference between benign and malignant breast lesions. Recently, a five-parameter empirical mathematical model (EMM) was developed to describe contrast uptake and washout behavior (20), and this model successfully distinguishes between benign and malignant lesions. Unfortunately, the EMM was performed with special protocols that allow acquisition of data with high temporal resolution, but are not clinically feasible (15,20). The limited temporal resolution in conventional 3D bilateral DCE-MRI implies that complicated mathematical models cannot be directly applied to kinetic curves to obtain a unique solution.

In this study a modified EMM with only three parameters was used to analyze 3D bilateral DCE-MRI breast data that was acquired according to clinical protocols, with sparse time resolution of 68 sec. Primary model parameters were determined by fitting the curves to the modified EMM. Secondary diagnostic parameters, such as initial area under curve (AUC_{30}) (21,22), initial slope of enhancement ($Slope_{ini}$) (10,21,23), the time to peak enhancement (T_{peak}) (10), signal enhancement ratio (SER) (11), and enhancement curvature at peak (κ_{peak}) (24) were derived mathematically from the primary parameters after fitting the kinetic curves. The sensitivity and specificity to malignant lesions using these parameters was also evaluated by using receiver operating characteristic (ROC) analysis and was compared to the kinetic curve classification according to the BI-RADS lexicon. In addition to comparing benign versus malignant lesions, the kinetic characteristics of subtypes of benign and malignant lesions were also studied.

MATERIALS AND METHODS

Patients

Diagnostic MR imaging is performed at this institution routinely for several clinical purposes: diagnostic imaging, evaluating extent of known disease, posttreatment, and surgical evaluation and as a screening tool in high-risk women. Bilateral 3D DCE-MRI data from 100 female patients was acquired consecutively between May 2002 and June 2003 and reviewed for study under an Institutional Review Board (IRB)-approved protocol, with informed consent waived and under full HIPAA compliance. The age range of the subjects

was 24 to 81 years (mean age = 56.2 ± 13.3 years). Based on the consensus opinion of two experienced pathologists, there were 34 benign and 79 malignant lesions used in this study.

MR Imaging

MR imaging was performed on a 1.5T GE Signa scanner (GE Healthcare, Milwaukee, WI) using a dedicated 4-channel breast coil (Invivo, Orlando, FL) with the patient in the prone position. One pre- and five postcontrast images were acquired in the coronal plane using a 3D T_1-weighted spoiled grass sequence (TR/TE = 7.7/4.2 ms, flip angle = 30°, slice thickness = 3 mm, and in-plane resolution = 1.4 mm) without fat saturation. The first postcontrast acquisition was started 20 sec after contrast injection and the remaining images were acquired every 68 sec. Gadodiamide (Omniscan; Nycomed-Amersham, Princeton, NJ) was injected intravenously at a dose of 0.1 mmol/kg followed by a 20-mL saline flush at the rate of 2.0 mL/sec.

All kinetic analysis was performed by experienced radiologists using coronal and reconstructed axial and sagittal views to assess the lesion. To generate the kinetic curve the radiologist traced a small region of interest (ROI) around what was perceived to be the most enhancing part of the lesion on the first postcontrast image. The average ROI size was 7.1 pixels; thus, the selected ROIs were small and contained the most enhancing contiguous pixels in the lesion as perceived by the radiologist. The plot of signal intensity versus time for this ROI was assessed by the radiologist according to the BI-RADS lexicon, which describes the “initial rise” and “delayed phase” of the kinetic curve. The “initial rise” is classified as rapid, medium, or slow. The “delayed phase” refers to the portion of the kinetic curve after 2 min and is classified as persistent (the signal intensity continues rise), plateau (the signal intensity levels off), and washout (the signal intensity decreases).

Modified EMM

The kinetic curve obtained above was analyzed quantitatively using the modified EMM (24). First, the average DCE-MRI signal intensity as a function of time ($S(t)$) in the selected ROI was calculated. Next, signal changes after contrast injection were calculated as: $\Delta S = (S_n - S_0)/S_0$, where S_0 is the average signal intensity within the ROI in the precontrast scan and S_n is the signal intensity within the ROI at the n^{th} postcontrast timepoint. The following modified EMM was used to describe the lesion contrast uptake and washout and to fit the data:

$$\Delta S(t) = A \cdot (1 - e^{-\alpha t}) \cdot e^{-\beta t}, \quad [1]$$

where A is the upper limit of the signal intensity, α (min^{-1}) is the rate of signal increase, β(min^{-1}) is the rate of the signal decrease during washout. The goodness of fit parameter R^2 was calculated for each lesion. The signal intensity modeled here is dependent on the noncontrast T_1 of the lesions. This is consistent with routine clinical practice, since radiologists typically evaluate changes in signal intensity following contrast injection. Variations in the native tissue T_1 values will affect the measured signal intensity; however, since T_1 values of benign and malignant lesions show considerable overlap (25–28), the results here may not be strongly affected.

Derived Diagnostic Parameters

Semiquantitative diagnostic parameters used commonly in the literature were easily derived from the modified EMM parameters. After some simple mathematical manipulations, we obtained the following derivations for diagnostic parameters: (a) Initial area under curve (AUC_τ): The AUC_τ can be calculated by integration of the kinetic curve, i.e.:

$$AUC_\tau = A \cdot [(1 - e^{-\beta\tau})/\beta + (e^{-(\alpha+\beta)\tau} - 1)/(\alpha+\beta)], \quad [2]$$

where τ is the time over which signal intensity was integrated. In this study we used $\tau = 30$ sec. (b) Initial slope of enhancement ($Slope_{ini}$): The initial slope of the kinetic curve can be calculated by taking the derivative of Eq. [1] at an initial time $t \ll 1$:

$$Slope_{ini} \approx A\alpha. \quad [3]$$

Thus, the initial slope is the product of the uptake rate α and the amplitude of enhancement A. (c) Time to peak of enhancement (T_{peak}): The time at which the kinetic curve reached peak can be solved by setting the derivative of Eq. [1] equal to zero:

$$T_{peak} = \frac{1}{\alpha}\log\left(1 + \frac{\alpha}{\beta}\right). \quad [4]$$

Please notice that when $\beta \leq 0$ the curves did not reach the peak within the duration of the experiment. In these cases, we used the last point as the peak intensity. (d) Signal enhancement ratio (SER): The signal intensity change at the first timepoint (ΔS_1) relative to the last time point (ΔS_L) was used to calculate the SER using the following formula:

$$SER = \frac{\Delta S_1}{\Delta S_L} = \frac{1 - e^{-\alpha t_1}}{1 - e^{-\alpha t_L}} \cdot e^{(t_L - t_1)\beta}, \quad [5]$$

where $t_1 = 60$ sec and $t_L = 300$ sec used in this study. A SER value greater than 1.1 indicates the signal intensity decreases with respect to its value at 60 sec; SER less than 0.9 indicates that signal intensity continues to rise; and SER between 0.9 and 1.1 represents a plateau relative to intensity at 60 sec. (e) Enhancement curvature at peak (κ_{peak}): The curvature at the peak of enhancement was calculated from the definition of curvature formula at time of T_{peak}:

$$\kappa_{peak} \approx -A\alpha\beta. \quad [6]$$

Data Analysis and Statistical Evaluation

For the qualitative evaluation according to the BI-RADS lexicon, distributions of initial rise and delayed phase were determined for benign and malignant lesions. To compare these distributions the chi-square (χ^2) test was used, with $P < 0.05$ indicating statistical significance.

The 3D bilateral DCE-MRI data were processed using software written in IDL (Research Systems, Boulder, CO). The average values of the diagnostic parameters were calculated separately for benign and malignant lesions. In addition, the benign and malignant lesions were further divided into pathologic subtypes. For malignant lesions these subtypes were: invasive ductal carcinoma (IDC), ductal carcinoma in situ (DCIS), invasive lobular carcinoma (ILC), and “other.” For benign lesions these subtypes were: fibrocystic change (FCC), fibroadenoma, papilloma, and “other.” Two-tailed unequal variance Student’s *t*-tests were performed to evaluate which parameters showed significant differences between the benign and malignant breast lesions, with $P < 0.05$ indicating statistical significance.

In order to determine whether modified EMM parameters varied within pathologic subtypes of benign and malignant lesions (for example, if the parameter α varied significantly among DCIS, ILC, and IDC lesions) ANOVA calculations were used, with $P < 0.05$ indicating statistical significance. The ANOVA analysis was performed on the three classified subtypes of malignant lesions (DCIS, ILC, and IDC) and the three classified subtypes of benign lesions (fibroadenoma, papilloma, and FCC). We also performed a multivariate analysis using a stepwise logistic regression algorithm in Matlab (MathWorks, Natick, MA) in order to determine whether a combination of primary and derived EMM parameters could better separate benign from malignant lesions. We used backwise regression (that is, the initial model included all parameters) and the minimum *P* value for removal of 0.1. Receiver operating characteristic (ROC) analysis was performed to compare the diagnostic capability of the parameters derived from the modified EMM with the diagnostic performance of the qualitative BI-RADS categories of initial rise and delayed phase. ROCKIT software (ROCKIT 0.9B Beta Version, Charles E. Metz, University of Chicago (29)) was used to generate the ROC curves and perform statistical comparisons between them via the bivariate and area test.

RESULTS

BI-RADS Classification

The distribution of initial uptake and delayed phase for all lesions as well as the breakdown of benign and malignant lesions into pathology subtypes is shown in Table 1. Malignant and benign lesions did not have statistically significantly different distributions of initial rise, but differed in delayed phase distribution with 65% and 38% showing washout curves, respectively ($P = 0.03$). Similarly, DCIS and IDC lesions were significantly different in delayed phase, with 50% and 78% showing washout, respectively ($P = 0.04$). Considering "washout" and "plateau" to be indicative of malignancy (10,13) the sensitivity and specificity were 91% (95% confidence interval [CI] 83–96%) and 18% (95% CI 7–35%), respectively. For initial phase criteria, considering "rapid" to be indicative of malignancy, the sensitivity and specificity were 89% (95% CI 79–95%) and 26% (95% CI 13–44%), respectively. In most prior studies of the kinetics of benign and malignant lesions, only IDC lesions were considered (10,13). When considering only the IDC lesions the sensitivity of "washout" and "plateau" as described in the BI-RADS lexicon improved to 97% (95% CI 85–100%), and the sensitivity of "rapid" improved to 92% (95% CI 78–98%).

Modified EMM Parameters

The modified EMM was able to accurately fit the curves, with a goodness of fit parameter R^2 greater than 0.90 for all cases studied here. Some typical examples of the modified EMM fits are shown in Fig. 1 for various benign (top row: FCC, fibroadenoma, and papilloma) and malignant lesions (bottom row: DCIS, IDC, and ILC). The distribution of the primary parameters for all the subcategories of benign and malignant lesions is shown in Fig. 2. Upon visual inspection substantial overlap between benign and malignant lesions was evident for the EMM parameters. After fitting all the kinetic curves the five derived diagnostic parameters were calculated using Eqs. [2–6].

The average values of all primary and derived parameters were calculated and are summarized in Table 2. From calculated averaged parameters it can be seen that malignant lesions had significantly faster contrast uptake (α), steeper initial slope ($Slope_{ini}$), larger enhancement ratio (SER), and sharper curvature (κ_{peak}) than benign lesions. Two-tailed unequal variance *t*-test showed that there was a statistically significant difference between benign and malignant lesions for the parameters of contrast uptake rate α ($P < 0.03$), initial slope $Slope_{ini}$ ($P < 0.04$), signal enhancement ratio SER ($P < 0.0007$), and the curvature at

the peak κ_{peak} ($P < 0.02$). To evaluate diagnostic performance ROC curves were generated for all parameters, with calculated A_z values shown in Fig. 3. The parameter A had the smallest area under the ROC curve (A_z), while SER had the largest. The ROC curves for the two parameters (Fig. 4) with the largest A_z values, α (blue line with solid square) and SER (red line with solid circle), are statistically equivalent under the bivariate and area test. From these ROC curves we can see that at a sensitivity of ≈90% the specificity was ≈20–30%, which was within the CI of the specificity achieved with the BI-RADS delayed phase and initial rise descriptors.

It is interesting to study further the kinetic properties of the subtypes of benign and malignant lesions. The calculated average values showed that the primary as well as diagnostic parameters for FCC were very similar to DCIS, which contributed to the majority of the overlap between the benign and malignant lesions. Performing *t*-test comparisons between these groups (DCIS vs. FCC) yields no statistically significant difference ($P > 0.06$ for all parameters). On the other hand, the contrast uptake and washout rates for IDC were much faster than benign lesions. As a result, IDC lesions had the largest AUC_{30}, deepest $Slope_{ini}$, highest SER, and sharpest κ_{peak}. In addition, for all primary and derived parameters there was a statistically significant difference (at least $P < 0.02$) between IDC and DCIS lesions. This suggests that the diagnostic accuracy of the modified EMM parameters may be improved if we consider only IDC lesions. To explore this, Fig. 4 also shows ROC curves (lines with open symbols) for α and SER when testing benign versus IDC lesions only. As shown in the figure, these ROC curves demonstrate considerable improvement in the A_z values compared to their benign versus all malignant lesions counterparts. At a sensitivity of ≈95% the specificity was ≈10–30%, which was within the CI achieved with the BI-RADS classifications.

To test whether a combination of parameters could improve the sensitivity and specificity, multivariate analysis was performed. However, the recommended model selected by backward stepwise regression included only the parameter SER. Based on these results it would seem that combinations of the EMM primary and derived parameters will not improve sensitivity and specificity.

Finally, ANOVA analysis was used to study the variation of the primary and derived parameters within benign and malignant subcategories. Three parameters (α, T_{peak}, SER) varied significantly by subtype for benign lesions ($P < 0.03$ for all), whereas all but one (*A*, α, T_{peak}, AUC_{30}, $Slope_{ini}$, κ_{peak}, SER) varied significantly for malignant subtypes ($P < 0.007$ for all).

DISCUSSION

In this study we found that 68% of malignant curves exhibited “washout,” which is similar to prior reports; however, 38% of benign curves also showed “washout,” which is higher than many reports (13). This may be because the benign lesions considered in this study were histologically proven benign—in other words, these lesions were suspicious enough to warrant biopsy. Since most obviously benign lesions have “persistent” type curves and would not be sent to biopsy, this may skew the delayed phase distribution in this study away from the “persistent” curve type. Szabo et al (10) considered only histologically proven benign lesions, and found that 24% of benign lesions showed “washout” type curves, a value closer to the one presented here. Because of the large number of benign lesions with “plateau” and “washout” type curves in this study, using these descriptors from the BI-RADS kinetic classification provided high sensitivity and low specificity in diagnosing malignant lesions.

The results demonstrated that the modified EMM fit the 3D DCE-MRI data very well for all cases. All the secondary diagnostic parameters could be easily calculated from the EMM parameters. Thus, we were able to calculate parameters, such as AUC_{30} and κ_{peak}, which could not be calculated directly from kinetic data comprised of only 6 points. The sensitivity and specificity of the BI-RADS delayed phase and initial rise classifications were 89–91% and 18–26%, respectively. Using the primary model parameter α or the derived parameter SER, at ≈90% sensitivity the specificity was ≈20–30%, which was not statistically different from the corresponding BI-RADS results. However, unlike the BI-RADS classification the EMM can be used to achieve a continuous spectrum of sensitivity and specificity. For example, at a sensitivity of ≈80% the specificity was ≈40%.

The diagnostic accuracy of the model parameters may be compromised by the relatively large number of DCIS and ILC lesions in this study, which showed significant overlap with benign lesions. Indeed, most other studies usually focus only on IDC lesions (10). We found that when considering benign versus IDC lesions only, the plateau and washout descriptors from the BI-RADS lexicon had sensitivity and specificity of 97% and 18%, respectively. Similarly, the rapid descriptor from the BI-RADS lexicon had sensitivity and specificity of 92% and 26%, respectively. The corresponding values for α and SER were comparable to the BI-RADS results. However, at a reasonable sensitivity of ≈80% the specificity of the model parameters improved greatly to ≈60%. The multivariate analysis did not yield a combination of parameters that improved results compared with individual parameters. This may be due to several factors; we have considered a small number of lesions and some parameters may depend on each other mathematically, which in turn may reflect a biological dependence. Further investigation of the relationship that EMM parameters have with each other and with the underlying biology of breast lesions is needed.

We have studied several subtypes of benign and malignant lesions, each having unique underlying biology. Fibroadenomas involve a proliferation of both epithelial and mesenchymal cells, and often present as encapsulated, well-circumscribed masses. Papillomas, on the other hand, grow confined in mammary milk ducts. FCC refers to a variety of benign mammary alterations, which are thought of as exaggerated physiological phenomena rather than diseases. These include proliferative lesions, such as intraductal hyperplasia, as well as fibrocystic disease. Moving to the malignant subtypes of cancer, ILCs involve cancer cells of lobular origin, which have invaded the surrounding stroma in a diffusely infiltrating fashion. IDCs, on the other hand, are cancer cells of ductal origin, which have well-defined but infiltrative margins. DCIS lesions are also cancer cells of ductal origin that are still confined to the mammary ducts.

The significant overlap of DCIS lesions with benign lesions may be related to similarities in the underlying biology and vasculature (30,31). Because DCIS is the earliest form of malignant breast disease, improving the detection of DCIS is important, and further investigation into the presentation of DCIS would be interesting (32). The ANOVA results in this study indicate that most of the modified EMM parameters varied significantly across the subtypes of DCIS, ILC, and IDC. Uptake and the sharpness and magnitude of washout tended to increase from DCIS to ILC to IDC. DCIS and IDC lesions showed the most difference in all parameters, with DCIS lesions having on average a much longer time to peak enhancement (3.6 min) compared with IDC lesions (2.0 min). On the other hand, only three parameters (SER, T_{peak}, α) showed significant variations among benign lesions; fibroadenomas exhibited a smaller uptake rate and much longer time to peak enhancement than papillomas.

The modified EMM does not make assumptions about the underlying physiology of the lesion. Some assumptions required by two-compartment or multicompartment models (15)

can lead to fitting errors and subsequent diagnostic errors. On the other hand, this lack of direct correspondence to identifiable physiologic or anatomic features is also the main disadvantage of the modified EMM approach. This problem can be addressed by deriving equations that connect parameters of the modified EMM to physiologic and anatomic parameters associated with various models (i.e., two or more compartment models). The parameters A, α, and β in the modified EMM can be directly compared with two-compartment models described in eqs. [13–16] of Armitage et al. (15). For example, to compare the EMM with the Tofts model described in eq. [13] of Armitage et al., it can be seen that the $A = Dv_eK^{trans}/V_p(K^{trans}-k_{out}v_e)$, $\beta = k_{out}$, and $\alpha + \beta = K^{trans}/v_e$, where D is the dose of administered contrast agent, v_e is the extravascular extracellular space volume fraction, K^{trans} is the transfer constant, V_p is the volume of the plasma, and k_{out} is the rate constant for contrast media elimination. With such relationships the empirical model can be related to a physiologically motivated model.

There are other limitations to this study:

- Sparse sampling may result in fitting errors. In particular, prior work has suggested that high temporal resolution was required to sample the kinetic curve uptake and transition part of uptake and washout accurately (24).
- Preclinical studies suggest that specificity is improved when the tail of the washout curve is sampled for at least 15 min; the curves studied here are truncated at about 6 min (20).
- Using signal intensity rather than contrast concentration may result in errors due to variability of the native T_1 of the tissue. However, in the present application of the EMM we used signal intensity rather than contrast concentration to follow conventional clinical practice and to minimize noise amplification.
- The present model does not account for variations in the arterial input function (AIF) and this omission can introduce variability and systematic error. The EMM is designed to analyze and accurately fit the signal intensity curves or contrast concentration versus time curves, and these are a function of the AIF and the tissue response to the AIF. The effect of AIF can be removed by deconvoluting it from the contrast concentration curves, so that an impulse response function can be obtained. Future work will focus on deriving deconvolution algorithms and developing mathematical models for the impulse response function.
- To characterize the kinetics of the lesion only a small ROI was used, which results in lower SNR. In addition, one small ROI may not be a reliable representation of the entire lesion, especially for heterogeneously enhancing lesions. Although the ROI was placed on the most rapidly enhancing area of the lesion, as is clinical practice, there is no guarantee this is the region of most diagnostic utility. Also, the ROI was chosen manually, resulting in variations in size and placement.
- Although the total number of lesions studied was relatively large, when considering subtypes of benign and malignant lesions (such as fibroadenoma or ILC) only a few cases were found, raising the issue of statistical validity. In particular, the numbers of lesions may be too small to perform reliable comparisons of the subtypes of benign and malignant lesions presented here.
- Recent parallel imaging techniques render the data we have used here slightly outdated, and the EMM will need to be tested with these new methods. We expect that the EMM will succeed with newer data, since the temporal resolution is comparable to that used in the studies described here. However, with the improved spatial resolution of parallel imaging, the ROI selection could likely be refined.

Despite the shortcomings summarized above, these results show that in our patient group, analysis of conventional 3D DCE-MRI data with the EMM provides at least the diagnostic accuracy of qualitative kinetic parameters described in the BI-RADS lexicon, and offers a few key advantages. It can be used to standardize kinetic data between institutions—currently, when radiologists are presented with an outside MRI for evaluation there is no way to relate the kinetic findings of the outside case to experience at the home institution. For example, if MR images at the outside institution are acquired every 90 sec, and at the home institution the dynamic protocol acquires images every 60 sec, the EMM can be used to present the outside kinetic data with 60-sec time resolution. The EMM can be automated and can provide a more objective classification. The EMM provides continuous variables so that thresholds can be set to achieve desired sensitivity and specificity. It also offers an opportunity to relate semiquantitative parameters (such as SER) to more fundamental EMM parameters. More important, this model allows for more flexibility in improving sensitivity and specificity in the future by correcting for AIFs. This model may become valuable as new protocols are being implemented at higher field strength and become more available. With the development of parallel imaging techniques it is now possible to acquire images with relatively high spatial resolution while still acquiring 6 or 7 kinetic data points. Thus, optimizing the diagnostic utility of kinetic data will be more and more important, and these preliminary results have demonstrated that the EMM may be useful for analysis of routine clinical data.

Acknowledgments

The authors thank Dr. Yulei Jiang and Ms. Marieke Heisen for assistance with statistical analysis.

Grant sponsor: Segal Foundation; Grant sponsor: Biological Sciences Division at the University of Chicago; Grant sponsor: Department of Defense; Grant number: W81XWH-06-1-0329; Grant sponsor: National Institutes of Health (NIH); Grant numbers: R21 CA104774-01A2 and 2 R01 CA078803-05A2.

References

1. Tabar L, Dean PB. Mammography and breast cancer: the new era. Int J Gynaecol Obstet. 2003; 82:319–326. [PubMed: 14499978]
2. Abraham DC, Jones RC, Jones SE, Cheek JH, Peters GN, Knox SM, Grant MD, Hampe DW, Savino DA, Harms SE. Evaluation of neoadjuvant chemotherapeutic response of locally advanced breast cancer by magnetic resonance imaging. Cancer. 1996; 78:91–100. [PubMed: 8646731]
3. Boetes C, Mus RD, Holland R, Barentsz JO, Strijk SP, Wobbes T, Hendriks JH, Ruys SH. Breast tumors: comparative accuracy of MR imaging relative to mammography and US for demonstrating extent. Radiology. 1995; 197:743–747. [PubMed: 7480749]
4. Warren RM, Pointon L, Thompson D, Hoff R, Gilbert FJ, Padhani A, Easton D, Lakhani SR, Leach MO. Reading protocol for dynamic contrast-enhanced MR images of the breast: sensitivity and specificity analysis. Radiology. 2005; 236:779–788. [PubMed: 16118160]
5. Heywang-Kobrunner SH, Bick U, Bradley WG Jr, Bone B, Casselman J, Coulthard A, Fischer U, Muller-Schimpfle M, Oellinger H, Patt R, Teubner J, Friedrich M, Newstead G, Holland R, Schauer A, Sickles EA, Tabar L, Waisman J, Wernecke KD. International investigation of breast MRI: results of a multicentre study (11 sites) concerning diagnostic parameters for contrast-enhanced MRI based on 519 histopathologically correlated lesions. Eur Radiol. 2001; 11:531–546. [PubMed: 11354744]
6. Orel SG. MR imaging of the breast. Radiol Clin North Am. 2000; 38:899–913. [PubMed: 10943285]
7. Kuhl CK, Schild HH, Morakkabati N. Dynamic bilateral contrast-enhanced MR imaging of the breast: trade-off between spatial and temporal resolution. Radiology. 2005; 236:789–800. [PubMed: 16118161]
8. Goto M, Ito H, Akazawa K, Kubota T, Kizu O, Yamada K, Nishimura T. Diagnosis of breast tumors by contrast-enhanced MR imaging: comparison between the diagnostic performance of dynamic

enhancement patterns and morphologic features. J Magn Reson Imaging. 2007; 25:104–112. [PubMed: 17152054]

9. Bazzocchi M, Zuiani C, Panizza P, Del Frate C, Soldano F, Isola M, Sardanelli F, Giuseppetti GM, Simonetti G, Lattanzio V, Del Maschio A. Contrast-enhanced breast MRI in patients with suspicious microcalcifications on mammography: results of a multicenter trial. AJR Am J Roentgenol. 2006; 186:1723–1732. [PubMed: 16714666]
10. Szabo BK, Aspelin P, Wiberg MK, Bone B. Dynamic MR imaging of the breast. Analysis of kinetic and morphologic diagnostic criteria. Acta Radiol. 2003; 44:379–386. [PubMed: 12846687]
11. Esserman L, Hylton N, George T, Weidner N. Contrast-enhanced magnetic resonance imaging to assess tumor histopathology and angiogenesis in breast carcinoma. Breast J. 1999; 5:13–21. [PubMed: 11348250]
12. Kuhl CK, Schild HH. Dynamic image interpretation of MRI of the breast. J Magn Reson Imaging. 2000; 12:965–974. [PubMed: 11105038]
13. Kuhl CK, Mielcareck P, Klaschik S, Leutner C, Wardelmann E, Gieseke J, Schild HH. Dynamic breast MR imaging: are signal intensity time course data useful for differential diagnosis of enhancing lesions? Radiology. 1999; 211:101–110. [PubMed: 10189459]
14. Cron GO, Kelcz F, Santyr GE. Improvement in breast lesion characterization with dynamic contrast-enhanced MRI using pharmacokinetic modeling and bookend T(1) measurements. Magn Reson Med. 2004; 51:1066–1070. [PubMed: 15122692]
15. Armitage P, Behrenbruch C, Brady M, Moore N. Extracting and visualizing physiological parameters using dynamic contrast-enhanced magnetic resonance imaging of the breast. Med Image Anal. 2005; 9:315–329. [PubMed: 15950895]
16. Furman-Haran E, Degani H. Parametric analysis of breast MRI. J Comput Assist Tomogr. 2002; 26:376–386. [PubMed: 12016367]
17. Furman-Haran E, Schechtman E, Kelcz F, Kirshenbaum K, Degani H. Magnetic resonance imaging reveals functional diversity of the vasculature in benign and malignant breast lesions. Cancer. 2005; 104:708–718. [PubMed: 15971199]
18. Tofts PS, Berkowitz B, Schnall MD. Quantitative analysis of dynamic Gd-DTPA enhancement in breast tumors using a permeability model. Magn Reson Med. 1995; 33:564–568. [PubMed: 7776889]
19. Heiberg EV, Perman WH, Herrmann VM, Janney CG. Dynamic sequential 3D gadolinium-enhanced MRI of the whole breast. Magn Reson Imaging. 1996; 14:337–348. [PubMed: 8782170]
20. Fan X, Medved M, River JN, Zamora M, Corot C, Robert P, Bourrinet P, Lipton M, Culp RM, Karczmar GS. New model for analysis of dynamic contrast-enhanced MRI data distinguishes metastatic from nonmetastatic transplanted rodent prostate tumors. Magn Reson Med. 2004; 51:487–494. [PubMed: 15004789]
21. Moate PJ, Dougherty L, Schnall MD, Landis RJ, Boston RC. A modified logistic model to describe gadolinium kinetics in breast tumors. Magn Reson Imaging. 2004; 22:467–473. [PubMed: 15120165]
22. Evelhoch JL. Key factors in the acquisition of contrast kinetic data for oncology. J Magn Reson Imaging. 1999; 10:254–259. [PubMed: 10508284]
23. Buadu LD, Murakami J, Murayama S, Hashiguchi N, Sakai S, Masuda K, Toyoshima S, Kuroki S, Ohno S. Breast lesions: correlation of contrast medium enhancement patterns on MR images with histopathologic findings and tumor angiogenesis. Radiology. 1996; 200:639–649. [PubMed: 8756909]
24. Fan X, Medved M, Karczmar GS, Yang C, Foxley S, Arkani S, Recant W, Zamora MA, Abe H, Newstead GM. Diagnosis of suspicious breast lesions using an empirical mathematical model for dynamic contrast-enhanced MRI. Magn Reson Imaging. 2007; 25:593–603. [PubMed: 17540270]
25. Kelcz F, Santyr GE, Cron GO, Mongin SJ. Application of a quantitative model to differentiate benign from malignant breast lesions detected by dynamic, gadolinium-enhanced MRI. J Magn Reson Imaging. 1996; 6:743–752. [PubMed: 8890012]
26. Callicott C, Thomas JM, Goode AW. The magnetization transfer characteristics of human breast tissues: an in vitro NMR study. Phys Med Biol. 1999; 44:1147–1154. [PubMed: 10368008]

27. Hulka CA, Smith BL, Sgroi DC, Tan L, Edmister WB, Semple JP, Campbell T, Kopans DB, Brady TJ, Weisskoff RM. Benign and malignant breast lesions: differentiation with echo-planar MR imaging. Radiology. 1995; 197:33–38. [PubMed: 7568850]

28. Jacobs MA, Barker PB, Bluemke DA, Maranto C, Arnold C, Herskovits EH, Bhujwalla Z. Benign and malignant breast lesions: diagnosis with multiparametric MR imaging. Radiology. 2003; 229:225–232. [PubMed: 14519877]

29. Metz CE, Herman BA, Shen JH. Maximum likelihood estimation of receiver operating characteristic (ROC) curves from continuously-distributed data. Stat Med. 1998; 17:1033–1053. [PubMed: 9612889]

30. Arpino G, Laucirica R, Elledge RM. Premalignant and in situ breast disease: biology and clinical implications. Ann Intern Med. 2005; 143:446–457. [PubMed: 16172443]

31. Kumar AS, Chen DF, Au A, Chen YY, Leung J, Garwood ER, Gibbs J, Hylton N, Esserman LJ. Biologic significance of false-positive magnetic resonance imaging enhancement in the setting of ductal carcinoma in situ. Am J Surg. 2006; 192:520–524. [PubMed: 16978965]

32. Jansen S, Newstead G, Abe H, Shimauchi A, Schmidt R, Karczmar GS. Pure ductal carcinoma in situ: kinetics, morphology and comparison with mammographic presentation and nuclear grade. Radiology. 2007; 245:684–691. [PubMed: 18024450]

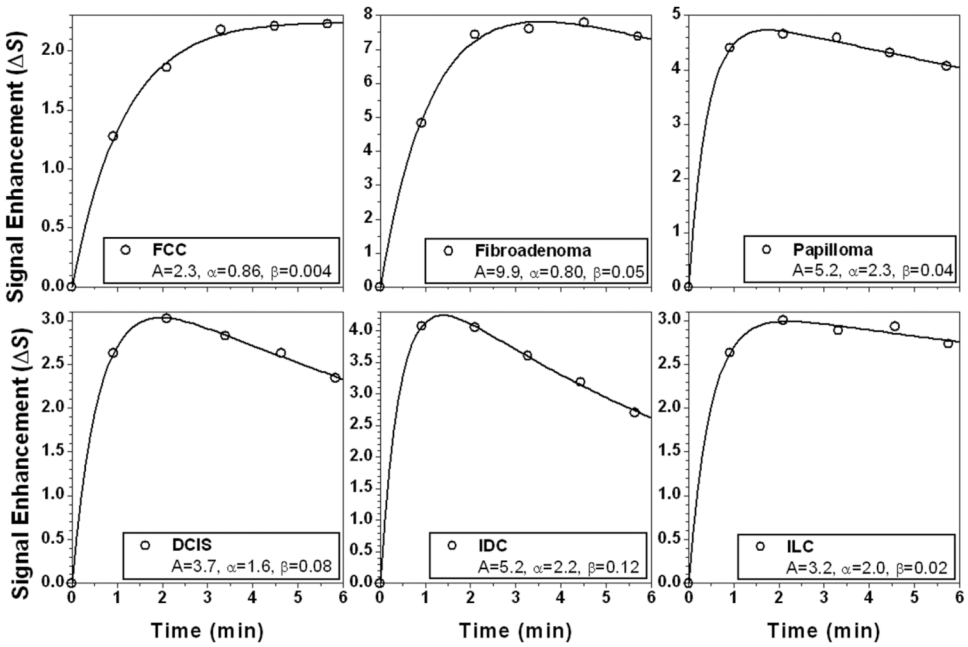

FIG. 1.

Examples of MRI signal enhancement versus time curves (open circles) are shown for a variety of lesion types and fitted with the modified EMM (solid lines). The top row consists of benign lesions, from left to right: fibrocystic change (FCC), fibroadenoma, and papilloma. The bottom row consists of malignant lesions, from left to right: ductal carcinoma in situ (DCIS), invasive ductal carcinoma (IDC), and invasive lobular carcinoma (ILC).

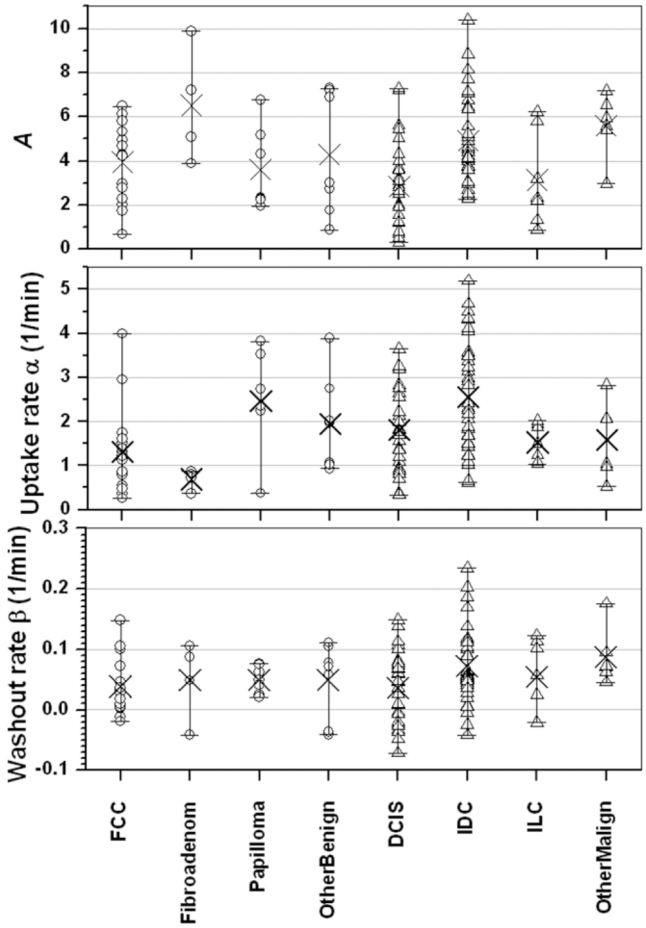

FIG. 2.

The distributions of the primary EMM parameters are shown according to lesion type. From top to bottom the primary EMM parameters are the amplitude *A*, the uptake rate α, and the washout rate β. The open circles display the values of the primary EMM parameter for every case in that subtype of benign lesion, and × marks the average value: fibrocystic change (FCC, $n = 16$), fibroadenoma ($n = 4$), papilloma ($n = 7$), and other benign ($n = 7$). Similarly, the open triangles represent the values of each primary EMM parameter for every case in that subtype of malignant lesion, and × marks the average value: ductal carcinoma in situ (DCIS, $n = 30$), invasive ductal carcinoma (IDC, $n = 36$), invasive lobular carcinoma (ILC, $n = 7$), and other malignant ($n = 6$).

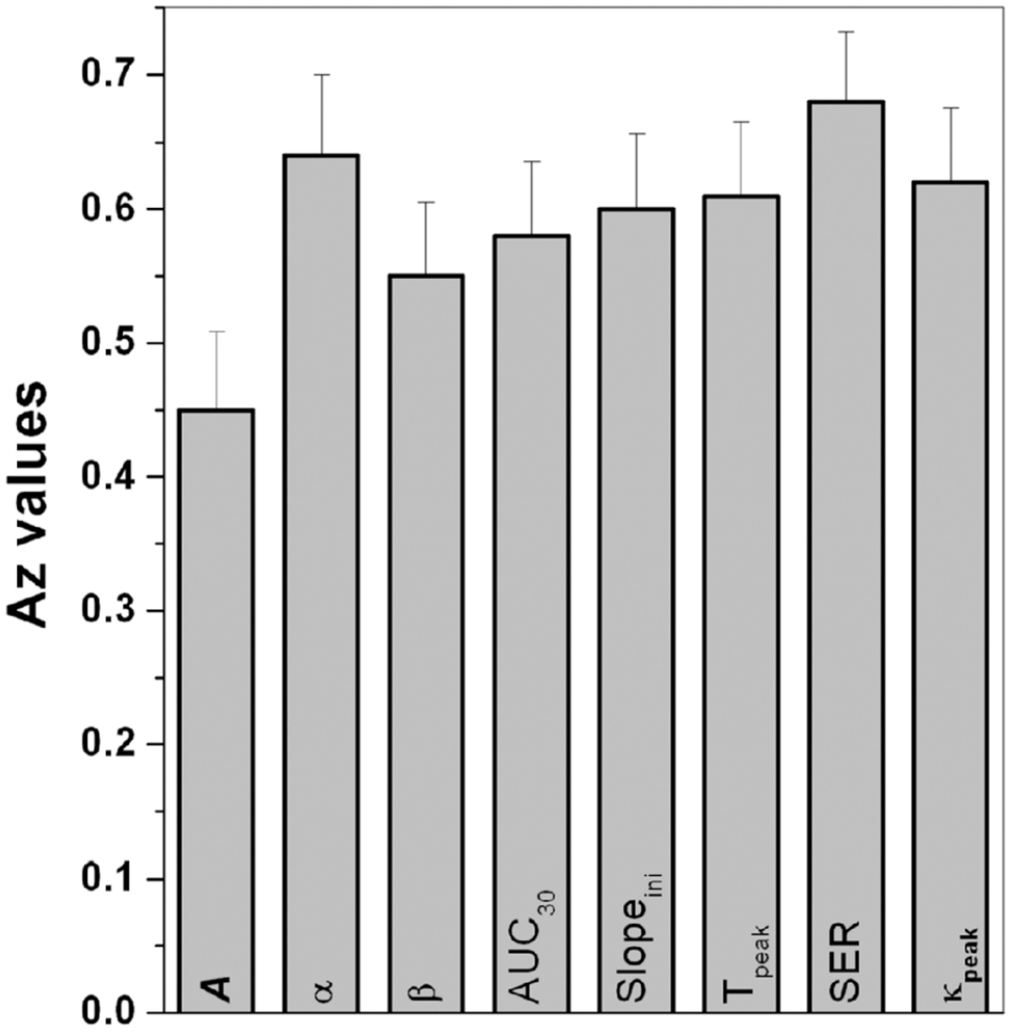

FIG. 3.

The bar graph of the area under the ROC curve (A_z) is shown for each EMM primary and derived parameter. The area under an ROC curve (A_z) gives a measure of how well the diagnostic parameter performs; the larger the area under the curve, the better the performance. The A_z values (and corresponding standard error) were determined from the fitted binormal ROC curves generated by the ROCKIT software. The standard errors are almost the same for all the cases.

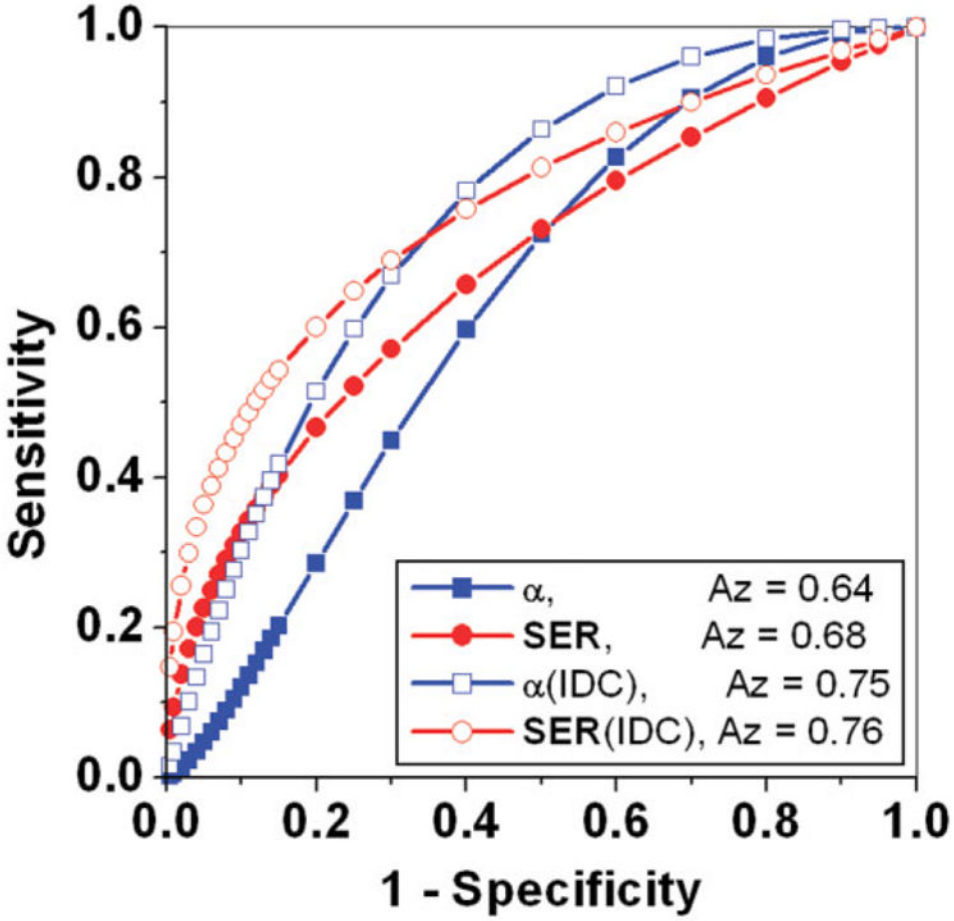

FIG. 4.

Fitted binormal ROC curves generated by the ROCKIT software are shown for selected parameters α (blue line with solid squares) and SER (red line with solid circles). The A_z values were improved by comparing benign lesions with IDC lesions only, as shown by the ROC curves for α (blue line with open squares) and SER (red line with open circles).

Table 1

Distributions of BI-RADS Categories for the Qualitative Assessment of the Initial Rise and Delayed Phased of Kinetic Curves for Benign and Malignant Lesions

Type of lesions	No. Cases	Initial			Delayed		
		Rapid	Medium	Slow	Washout	Plateau	Persistent
All benign	34	25 (74%)	8 (24%)	1 (3%)	13 (38%)	15 (44%)	6 (18%)
FCC	16	11	4	1	3	11	2
Fibroadenoma	4	2	2	0	2	1	1
Papilloma	7	6	1	0	4	2	1
Others	7	6	1	0	4	1	2
All malignant	79	70 (89%)	7 (9%)	2 (3%)	51 (65%)	21 (27%)	7 (9%)
DCIS	30	26	3	1	15	10	5
IDC	36	33	3	0	28	7	1
ILC	7	6	0	1	4	2	1
Others	6	5	1	0	4	2	0

Numbers in parentheses are percentages.

Table 2

Primary and Secondary Diagnostic Parameters Derived from the EMM in Malignant and Benign Lesions

Type of Lesions	No. Cases	*A*	α (min^{-1})	β (min^{-1})	AUC_{30}	$Slope_{ini}$ (min^{-1})	T_{peak} (min)*	κ_{peak}	SER
All benign	34	4.2 ± 2.2	**1.6 ± 1.1**	0.045 ± 0.047	0.55 ± 0.35	**6.1 ± 4.6**	3.4 ± 1.8	**30.30 ± 0.49**	**0.88 ± 0.30**
FCC	16	3.9 ± 1.8	1.3 ± 1.0	0.039 ± 0.046	0.48 ± 0.39	5.3 ± 5.5	4.0 ± 1.6	30.23 ± 0.56	0.78 ± 0.28
Fibroadenoma	4	6.5 ± 2.6	0.69 ± 0.22	0.050 ± 0.066	0.48 ± 0.25	4.4 ± 2.4	4.2 ± 1.4	30.22 ± 0.25	0.65 ± 0.19
Papilloma	7	3.6 ± 1.9	2.5 ± 1.1	0.050 ± 0.022	0.62 ± 0.28	7.5 ± 3.6	2.0 ± 1.2	30.33 ± 0.14	1.08 ± 0.7
Others	7	4.3 ± 2.8	2.0 ± 1.1	0.050 ± 0.063	0.66 ± 0.36	7.4 ± 4.4	3.2 ± 2.0	30.45 ± 0.64	1.04 ± 0.30
All malignant	79	4.0 ± 2.2	**2.1 ± 1.1**	0.058 ± 0.061	0.71 ± 0.54	**8.7 ± 8.3**	2.8 ± 1.9	**30.67 ± 1.18**	**1.14 ± 0.48**
DCIS	30	2.8 ± 1.9	1.8 ± 0.9	0.037 ± 0.058	0.40 ± 0.23	4.3 ± 2.6	3.6 ± 2.0	30.18 ± 0.31	0.96 ± 0.35
IDC	36	4.9 ± 2.0	2.6 ± 1.3	0.072 ± 0.062	1.01 ± 0.62	13.1 ± 10.2	2.0 ± 1.5	31.12 ± 1.57	1.31 ± 0.55
ILC	7	3.1 ± 2.1	1.5 ± 0.4	0.054 ± 0.062	0.44 ± 0.26	4.6 ± 2.7	3.2 ± 2.0	30.35 ± 0.40	1.04 ± 0.30
Others	6	5.6 ± 1.4	1.6 ± 0.9	0.087 ± 0.046	0.78 ± 0.38	8.5 ± 4.7	2.3 ± 1.0	30.82 ± 0.89	1.14 ± 0.57

Reported values are mean ± standard deviation for all cases. Numbers in bold indicate that there was a statistically significant difference between benign and malignant lesions.

*For those curves which did not reach a peak within the duration of the experiment, we assumed a time to peak of 5 min.